Solar-Terrestrial Physics. 2019. Vol. 5. Iss. 3. P. 98–108. DOI: 10.12737/stp-53201912. © 2019 Gubenko V.N., Kirillovich I.A. Published by INFRA-M Academic Publishing House
Original Russian version: Gubenko V.N., Kirillovich I.A., published in Solnechno-zemnaya fizika. 2019. Vol. 5. Iss. 3. P. 116–129. DOI: 10.12737/szf-53201912. © 2019 INFRA-M Academic Publishing House (Nauchno-Izdatelskii Tsentr INFRA-M)

MODULATION OF SPORADIC E LAYERS BY SMALL-SCALE ATMOSPHERIC WAVES IN EARTH'S HIGH-LATITUDE IONOSPHERE

V.N. Gubenko
Kotel'nikov Institute of Radioengineering and Electronics RAS, Fryazino, Russia, vngubenko@gmail.com

I.A. Kirillovich
Kotel'nikov Institute of Radioengineering and Electronics RAS, Fryazino, Russia, sabersecretmail@gmail.com

Abstract. We have used radio occultation measurements of the satellite CHAMP (Challenging Minisatellite Payload) to examine sporadic E layers in Earth's high-latitude ionosphere. The study of these thin layers of increased ionization, located in an altitude range 90–130 km, is of great interest for radio communications and navigation. We have developed a new method for determining characteristics of internal atmospheric waves based on the use of inclined sporadic E layers of Earth's ionosphere as a detector. The method relies on the fact that an internal wave propagating through the initially horizontal sporadic E layer causes the plasma density gradient to rotate in the direction of the wave vector, which leads to the fact that the layer ionization plane is set parallel to the phase wave front. The developed method enables us to study the interrelations between small-scale internal waves and sporadic E layers in Earth's ionosphere and significantly expands the capabilities of traditional radio occultation monitoring of the atmosphere. We have found that the internal atmospheric waves under study have periods from 35 to 46 min and vertical phase speeds from 1.2 to 2.0 m/s, which are in good agreement with the results of independent experiments and simulation data on sporadic E layers at a height of ~100 km in Earth's polar cap.

Keywords: radio occultation measurements, Earth's atmosphere and ionosphere, inclined sporadic E layers, internal atmospheric waves.

INTRODUCTION

Sporadic E layers (E_s) are thin layers of increased ionization at altitudes from 90 to 130 km in Earth's ionosphere. The study of the effects associated with E_s structures is important for ensuring smooth operation of radio communication and navigation systems. Analyzing radio occultation (RO) measurements of the CHAMP (Challenging Minisatellite Payload) satellite, Wu et al. [2005] have studied the global morphology of E_s layers. They examined the climatology of E_s layers by determining SNR (signal-to-noise ratio) and phase variances in terms of zonal monthly averages, seasonal maps, diurnal and long-term variations [Wu et al., 2005]. The global distribution of occurrence of E_s layers has been analyzed in detail by Arras et al. [2008]. To gain information on small-scale ionospheric irregularities, the authors have used a large database of radio occultation missions CHAMP, GRACE, and FORMOSAT-3/COSMIC for the period from January 2002 to December 2007. The distribution of occurrence of E_s layers has been shown to feature strong fluctuations, with the highest frequency of their occurrence at middle latitudes in summer. The maximum frequency of occurrence of irregularities is observed in geomagnetic latitudes from 10° to 60° of Earth's mid-latitude ionosphere. At high latitudes, where angles of magnetic inclination range from 70° to 80°, this distribution features deep minima, which agrees with the wind shear theory of the sporadic E-layer formation [Arras et al., 2008; Haldoupis, 2011].

The wind shear theory of E_s-layer formation at middle latitudes has been confirmed by many studies [Whitehead, 1989]. It has been found that the E_s layers at middle latitudes are very thin (their thickness is several hundred meters), distributed horizontally over hundreds of kilometers, dense (with density as high as several units $\times 10^6$ cm^{-3}), and consist of metal atoms [Kirkwood, Nilsson, 2000]. In the presence of inclined geomagnetic fields, ion coalescence in the E-region of the ionosphere can be caused by shear of both zonal and meridional winds. The zonal wind shear is, however, considered as the primary driver of ion convergence in midlatitudes at altitudes of ~ 115 km and below [Haldoupis, 2012]. Electrons associated with the coalescence of positive ions into a thin layer move along geomagnetic field lines to neutralize the positive charge. Note that the wind shear theory explains how the layer is formed in the vertical plane, but does not explain the principle of its formation in the horizontal plane. In the daytime E-region of the ionosphere, ionization largely involves N_2 and O_2 molecules. At night, fast recombination of the molecules leads to photochemical ionization equilibrium in this region, which is responsible for the disappearance of the ordinary E layer. Sporadic E layers are, however, often observed at night and usually for several hours. This contradicts the photochemical equilibrium of the ordinary E-region of the ionosphere and excludes its participation in the formation of positive ions responsible for ionization of E_s layers. To confirm the assumption that these are metal ions (Fe^+ and Mg^+) that make up a major source of ionization of E_s layers, electron and ion density profiles were directly measured using rocket observations [Roddy et al., 2004]. The theory predicts that recombination rates for these metal ions are considerably lower

than those for NO^+ and O_2^+. The lifetime of the metal ions is long and varies from a few days at an altitude of ~120 km to several hours at ~95 km [Haldoupis, 2012]. The metal atoms are very likely to have meteoric origin, so it is natural to assume that the thin sporadic layers are formed due to ion convergence caused by the impact of neutral wind shear in the presence of the geomagnetic field. While some observations of dense E_s layers detect meteors captured in wind shear nodes, the main mechanisms for the formation of the sporadic layers are considered to be neutral wind shears [Maruyama et al., 2003, 2008; Malhotra et al., 2008].

Nighttime ground-based radar observations allowed successful representation of the horizontal structure of E_s layers [Hysell et al., 2002, 2004; Larsen et al., 2007]. Numerical simulation has shown that the E_s layers in the Northern Hemisphere move southwestward, and, as a rule, extend from northwest to southeast [Cosgrove, Tsunoda, 2002, 2004; Yokoyama et al., 2009]. We, however, need a larger amount of observations of E_s layers at middle latitudes to justify the simulation results. In the presence of vertical wind shear, the main mechanisms for structuring E_s layers are: internal gravity waves (IGWs) [Woodman et al., 1991; Didebulidze, Lomidze, 2010; Chu et al, 2011], neutral wind shear instability [Larsen, 2000; Bernhardt, 2002; Larsen et al., 2007; Hysell et al., 2009], Es-layer plasma instability caused by neutral wind shear [Cosgrove, Tsunoda, 2002, 2004]. Internal atmospheric waves modulate E_s layers in the vertical direction, which may be a cause of quasiperiodic (QP) radar echoes. Tsunoda et al. [1994] have shown that due to the layer height modulation in the nightside mid-latitude ionosphere a polarization electric field develops, with polarization effects resembling atmospheric waves. The use of coherent scatter radars in modern ionospheric experiments provided a clear picture of structuring of ionization layers at midlatitudes [Yamamoto et al., 1991, 1992]. Rocket experiments have shown that quasiperiodic echoes are reflected from E_s layers in the presence of strong polarization electric fields and neutral wind shears [Bernhardt et al., 2005; Yamamoto et al., 2005]. Large wind shears did occur in two rocket experiments, which were conducted in parallel with ground-based radar observations (SEEK and SEEK-2) of E_s layers in the ionosphere over Kyushu [Larsen et al., 1998, 2005; Yokoyama et al., 2005]. Shear instability in the neutral atmosphere is also considered as a mechanism for creating a densely ionized structure of billows [Bernhardt, 2002]. In the rocket experiment carried out during the SEEK-2 campaign, such a structure of billows in the E-region of the ionosphere was displayed as a trace of trimethylaluminum (TMA) [Larsen et al., 2005]. Observations of three-dimensional structures of downward and approaching echoes [Saito et al., 2006] can be attributed to the presence of unstable regions, which developed along the geomagnetic field line from E_s-layer heights to higher levels (>120 km). The interferometer measurements made in the study [Saito et al., 2006] support the model proposed in [Maruyama et al., 2000; Ogawa et al., 2002] and confirm computer simulation results [Yokoyama et al., 2004].

At high latitudes (>60°), since the magnetic field is directed almost vertically to the local horizon, the mechanism for E_s-layer formation through wind shear is not as effective as that at middle latitudes. The large-scale horizontal plasma structure in the auroral E-region is determined by the spatial distribution of sources of solar radiation and particle precipitation. Internal atmospheric waves at high latitudes are less important as the mechanism for vertical structuring of the layers due to a large angle (~90°) of magnetic field inclination with respect to the local horizon [Kelley, 2009]. Nevertheless, the small angle of magnetic field inclination from vertical is very considerable here due to the large electric fields perpendicular to the magnetic field. At high latitudes, convective electric fields are important drivers of ion convergence or divergence [Nygren et al., 1984; Turunen et al., 1993; Bristow, Watkins, 1991, 1993; Kirkwood, von Zahn, 1991, 1993; Kirkwood, Nilsson, 2000]. Nygren et al. [1984] have first assumed that E_s layers may be formed by the impact of only one electric field at high latitudes, where the wind shear mechanism almost does not work, particularly at altitudes below 110 km. The electric field in the auroral zone and polar cap is much larger than that in the equatorial region and is more widely distributed over area. The mean auroral electric field has a strong diurnal component with an amplitude of 30 mV/m and maxima located near 5:00 and 18:00 LT. The field strength of ~50 mV/m is common both for the auroral oval and for the polar cap. Numerous measurements have also been reported in which the electric field strength exceeded 100 mV/m [Kelley, 2009]. There are clear signatures of the influence of tidal winds (semidiurnal and diurnal modes) on the formation of sporadic layers (electric fields are not included), but internal atmospheric waves can also produce additional wind nodes [Turunen et al., 1993]. In fact, Lehmacher et al. [2015] have shown that under very quiet conditions at auroral latitudes minimum electric fields by means of wind shear can form sporadic E layers. The results obtained in [Cox, Plane, 1998] indicate that at high latitudes E_s layers with a density of $\sim 3 \cdot 10^6$ cm^{-3} are often observed and there are a sufficient number of Na^+ ions to derive Na-atom densities measured in the experiments. Composition of metal ions in E_s layers suggests their connection with meteor ablation [Hunten et al., 1980] and with the formation of layers of neutral metal atoms in the upper mesosphere [Kirkwood, von Zahn, 1991, 1993; Heinselman et al., 1998]. Since the vertical speed is proportional to the cosine of the angle of magnetic field inclination with respect to the local horizon that is 0.034 for the inclination angle of 88°, which is significantly less than 0.17 for an angle of 80° [Kelley, 2009], the mechanisms involving horizontal electric fields or neutral winds do not work in the polar cap. The high-latitude E_s layers are assumed to be a manifestation of aurora, which is a powerful source of increased ionization. In this case, however, the sporadic layers are not very thin. According to the results obtained in [Kirkwood, Nilsson, 2000], at high latitudes there are sporadic layers of several types that are much thinner than those produced by auroral precipitation and are probably

formed by methods characteristic of the formation of the E_s layers at middle latitudes.

The purpose of this work is: a) to present a method for determining the location and inclination of plasma layers from radio occultation data; b) to observe inclined E_s layers in Earth's high-latitude ionosphere with the CHAMP satellite; c) to demonstrate a new method for determining characteristics of IGWs responsible for E_s-layer inclinations.

DETERMINING THE LOCATION OF E_S LAYERS AND THEIR INCLINATION WITH RESPECT TO THE LOCAL HORIZON FROM RADIO OCCULTATION DATA

A diagram of a radio occultation experiment is shown in Figure 1. Highly stable radio signals emitted by a transmitter, installed in a satellite G, passes through the ionosphere and atmosphere along a GTL ray and are recorded by a receiver on board a low-orbit satellite L. The amplitude $A(t)$ and the phase-path increase (eikonal) $\Phi(t)$ are measured at the carrier frequency. The global spherical symmetry of the ionosphere and atmosphere with a common center (point O in Figure 1) is a key assumption in the analysis of radio occultation data. The main contribution to variations in the amplitude and phase of a recorded signal is made by a small region near the tangential point T (where the radio ray is perpendicular to the refractive index gradient), despite the fact that the length of the ray trajectory GTL is much greater the length of the region [Igarashi et al., 2001]. The length of the indicated region on the ray trajectory $\Delta_h = 2\,(2l_f r_e)^{1/2}$. Here $l_f = (\lambda d_2)^{1/2}$ is the vertical size (radius) of the Fresnel zone; λ is the radio signal wavelength; r_e is the distance OT from the center O of the spherical symmetry of medium to the ray perigee T; d_2 is the length of the ray trajectory segment TL approximately equal to the length of the line segment DL (Figure 1). The value Δ_h is the minimum length of the horizontal layer, which can be measured by a radio occultation method, i.e. it in fact characterizes the horizontal resolution of the structure under study in the radio occultation experiment. The tangential point at which GTL is perpendicular to the refractive index gradient coincides with the ray perigee T in case of global spherical symmetry. The radio occultation method allows us to determine the refractive index and its vertical gradient along the ray perigee trajectory with high accuracy and high vertical resolution.

The relationship between eikonal acceleration a and refractive attenuation $X_p(t)$ of the RO signal has the form [Pavelyev et al., 2009, 2012, 2015]:

$$1-X_p(t)=ma,\ a=\mathrm{d}^2\Phi(t)/\mathrm{d}t^2,$$
$$m=d_1d_2/(R_0^{1/2}\,\mathrm{d}p_s/\mathrm{d}t)^2,\ d_1=R_0-d_2, \quad (1)$$

where d_1, d_2, and R_0 are the lengths of GD, DL, and GDL respectively, and p and p_s are the impact parameters for the ray trajectory GTL and the line of sight GDL. The m value is determined from ballistic data. Since the refractive angle $\xi(p)$ (Figure 1) is small, the distance d_2 is approximately equal to the TL arc length.

Formulate the conditions under which the tangential point coincides with the ray perigee: I) global spherical symmetry of the atmosphere and ionosphere, II) absence of random irregularities and multipath propagation of radio waves. Then Equation (1) holds, which leads to the identity of refractive attenuations X_a and X_p, determined from RO-signal amplitude and phase measurements:

$$X_p(t) \equiv X_a(t),\ X_a(t) = I / I_0, \quad (2)$$

where I_0 and I are the radio wave intensities recorded before and after the entry of the ray into the ionosphere. When relation (2) works, the tangential point of the ionospheric layer coincides with the ray perigee T. It is convenient to represent the refractive attenuations $X_p(t)$ and $X_a(t)$, determined from RO-signal eikonal and amplitude measurements, as analytical functions with amplitudes $A_p(t)$, $A_a(t)$ and phases $\chi_p(t)$, $\chi_a(t)$:

$$1 - X_p(t) = ma = A_p(t)\ \mathrm{Re}\ \exp[\,j\,\chi_p(t)],$$
$$1 - X_a(t) = ma = A_a(t)\ \mathrm{Re}\ \exp[\,j\,\chi_a(t)]. \quad (3)$$

The amplitudes $A_p(t)$, $A_a(t)$ and phases $\chi_p(t)$, $\chi_a(t)$ can be found from the known time dependence $1 - X_p(t)$ and $1 - X_a(t)$, e.g. using the numerical Hilbert transform or other methods of experimental data processing. In case of synchronous variations $1 - X_p(t)$ and $1 - X_a(t)$, Equation (1) yields:

$$A_p(t) = A_a(t),\ \chi_p(t) = \chi_a(t). \quad (4)$$

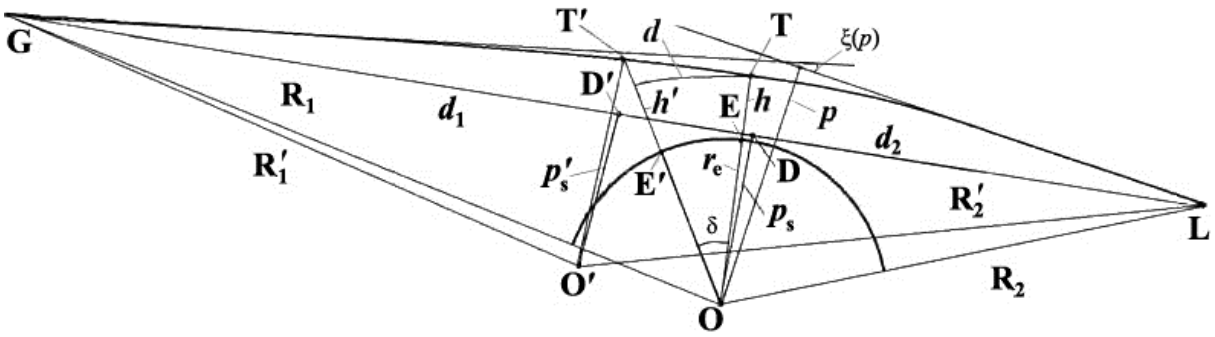

Figure 1. Diagram of a radio occultation experiment in Earth's ionosphere: G is the GPS satellite (highly stable radio transmitter); L is the low-orbit satellite CHAMP (receiver); GTL is the probing ray trajectory; T is the radio ray perigee; h = TE is the ray perigee height; $\xi(p)$ is the radio ray refractive angle; p and p_s = OD are the impact parameters for the ray trajectory GTL and the line of sight GDL respectively; d_1, d_2, and R_0 are the GD, DL, and GL distances respectively; R_1 and R_2 are the OG and OL distances respectively; h' =T′E′ is the actual layer height; δ is the angle of layer inclination with respect to the local horizon

When the condition of global spherical symmetry holds, Equation (4) represents the above condition given in another form. Deviations from it can be associated with multipath propagation, diffraction, and scattering of radio waves, as well as with the influence of turbulence and other irregularities in the atmosphere and ionosphere. In some cases, these deviations are due to horizontal gradients and appearance of other tangential points in ionospheric parts of radio ray, for example, of the tangential point T′ that causes the spherical symmetry center to displace from O to O′ (Figure 1).

The relationship for the displacement d of tangential point T′ relative to the ray perigee T has the following form [Pavelyev et al., 2012, 2015; Gubenko et al., 2018]:

$$d = d_2 \frac{A_a - A_p}{A_p}, \; d_2 = \sqrt{R_2^2 - p_s^2}. \quad (5)$$

From Equation (5) it follows that the displacement of the tangential (turning) point of ray trajectory is defined by the amplitudes A_a and A_p, which can be obtained from an analysis of RO-signal intensity and eikonal variations. Depending on the sign of the difference $(A_a - A_p)$, d is positive or negative, hence the tangential point T′ will be located on TL or TG respectively. In this case, $\chi_p(t)$ and $\chi_a(t)$ should be identical within the accuracy determined by measurement errors. Equation (5) is valid if one of the satellites is located at a much greater distance from the perigee point T than the other. This condition is met in the radio occultation experiments that use communication lines spaceship–Earth or when low-orbit satellites working with radio signals from space navigation systems are employed. If d is known, then we can find the correction Δh to calculate the actual layer height (h') and determine the angle of layer inclination δ with respect to the local horizon [Gubenko et al., 2018]:

$$\delta = d/r_e, \; \Delta h = h' - h = d\,\delta/2 = d^2/(2r_e), \quad (6)$$

where h is the ray perigee height (Figure 1).

ANALYZING CHAMP RADIO OCCULTATION DATA IN EARTH'S HIGH-LATITUDE IONOSPHERE

We have used CHAMP radio occultation measurements to study E_s layers in Earth's ionosphere. Figure 2 shows the results of the determination of the location and inclination of ionospheric layers as derived from radio signal processing at a frequency f_1=1575.42 MHz of the global positioning system (July 28, 2003, 01:35 UT; ray perigee coordinates 71.4° N, 67.3° W) in measurement session No. 13. Parameters of the ionospheric structures were determined by analyzing vertical variations of RO-signal phase path and intensity. This allowed us to estimate the spatial displacement of plasma structures with respect to the radio ray perigee, to determine angles of layer inclination with respect to the local horizon, and to find actual layer heights.

The time resolution of phase and intensity measurements of the radio signal received by CHAMP is 0.02 s, which corresponds to a sampling frequency of 50 Hz. The analyzed data indicates the presence of significant quasi-regular variations in radio wave intensity and phase. The refractive attenuations X_a and X_p of the RO signal obtained from processing of intensity and eikonal variations are presented in Figure 2, I (curves 1 and 2) as function of perigee height h for the ray trajectory GTL. The refraction attenuation X_p was found from Equation (1) by using values of the parameter a, determined from experimental data. The value m was calculated from ballistic data. We found X_a from measurements of the intensity of the RO signal received by CHAMP.

Variations in X_a and X_p are coherent, which indicates the equality of χ_a and χ_p. It is evident that these variations are caused by the influence of the ionospheric layers in three intervals of the GTL perigee height (a, b, and c in Figure 2, I). The intervals a, b, and c correspond to ranges of the ray perigee height: 50–72, 72–92, and 92–116 km. The functions $(X_a - 1)$ and $(X_p - 1)$ are seen to be coherent at the indicated intervals. The amplitudes A_a and A_p of the analytic functions $(X_a - 1)$ and $(X_p - 1)$ are, however, different. A_a (curve 1, Figure 2, II) and A_p (curve 2, Figure 2, II) were determined using the numerical Hilbert transform. The maximum values of A_a are less than the corresponding values of A_p in the intervals a and b (Figure 2, II). The opposite situation occurs in the interval c (Figure 2, I, II). For the layers in the intervals a and b, the displacement d is negative. These two layers are located on the ray trajectory GTL between the points T and L. The upper layer from the interval c is displaced from the ray perigee T to the navigation satellite G (Figure 1). For the case of non-zero layer displacement, the actual layer height h' and the ray perigee height h are not equal and differ by Δh, derived from Equation (6). It is important to note that the vertical position of the layer is not uniquely determined by h. For example, in accordance with Equation (6), two layers with the same ray perigee height h but different displacements d have unequal actual heights h'. The actual layer height is, therefore, a more adequate parameter for describing the height position of layer than the ray perigee height.

In radio occultation studies of Earth's ionosphere, not only discrete (single) E_s layers were observed but also more complex structures such as double E_s peaks and even rectangular sporadic layers [Yue et al., 2015]. The complex E_s layers can be caused by unstable wind shears. Bernhardt [2002] has shown that the drivers that contribute to plasma instability (e.g., Kelvin–Helmholtz instability) deform a discrete E_s layer and convert it into a complex structure. These drivers can lift a part of the E_s layer until it overlaps the original layer [Yue et al., 2015]. Referring to Figure 2, I, the layer in the interval a has a complex (double) quasiperiodic structure. The observed vertical signal oscillations perhaps indicate IGW propagation through the layer.

The lower part of this layer assigned to a ray perigee height of 55 km has a vertical size of 3.0 km, and the vertical size of its upper part assigned to a ray perigee height of 59 km is 4.4 km. A discrete sporadic layer b assigned to a ray perigee height of 85 km has a vertical size of 4.4 km and a typical U-shape structure, which was reported in [Zeng, Sokolovskiy, 2010], with oscillations

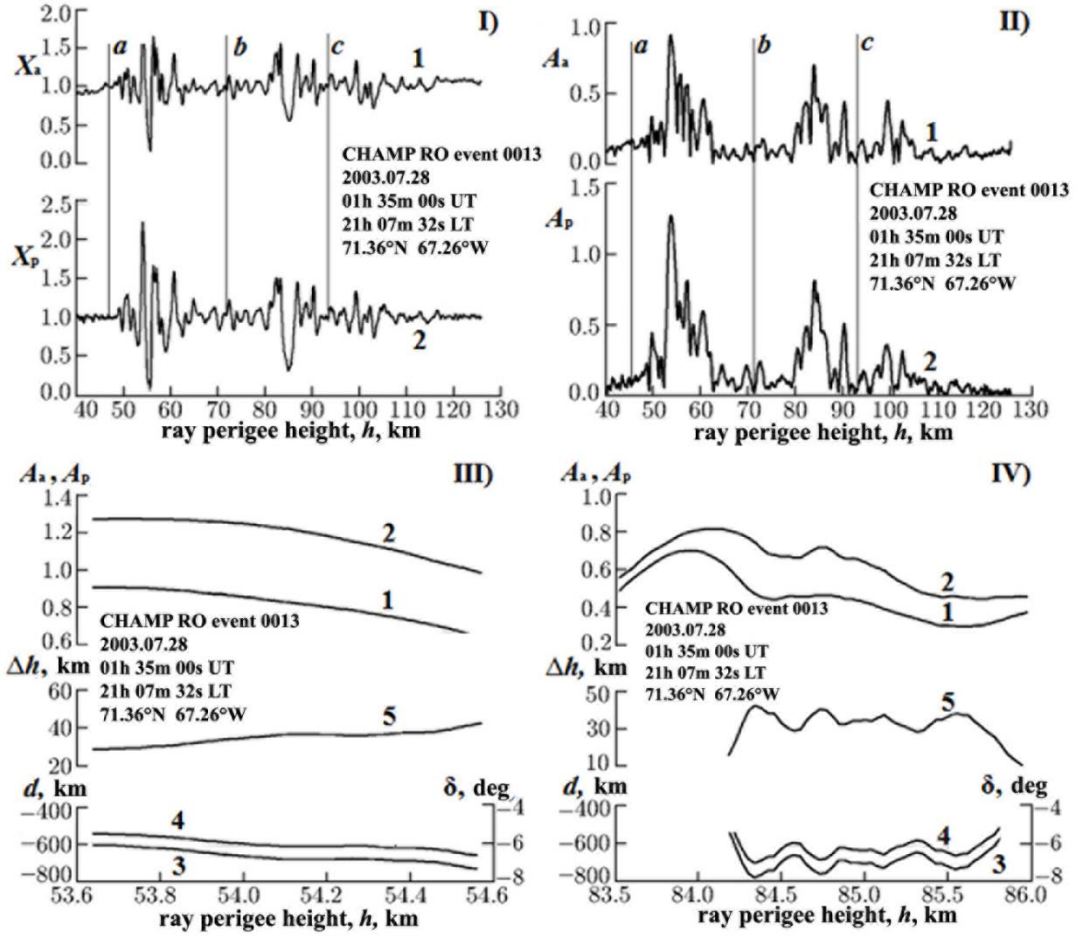

Figure 2. Refractive attenuations X_a and X_p, obtained from the CHAMP RO signal intensity and eikonal variations at a GPS frequency f_1=1575.42 MHz (curves 1 and 2 in panel I) in measurement session No. 13. Amplitudes A_a and A_p (curves 1 and 2 in panel II) of analytical signals associated with variations in X_a and X_p. Determination of the location and inclination of layers *a* (panel III) and *b* (panel IV) from A_a and A_p: curves 1, 2, 3 are dependences of A_a, A_p, and *d* on the ray perigee height; curve 4 shows angles of layer inclination δ; curve 5 is the correction for the actual layer height *h′*

above and below the defocusing region, which are caused by interference of direct and refracted radio rays. The layer of the interval *c* assigned to a ray perigee height of 103 km has a vertical size of 3.0 km. Figure 2, I shows that this layer is less pronounced than those located in the intervals *a* and *b*.

Since X_a and X_p variations are coherent, we can determine the location of the ionospheric layer on GTL. Results of the determination of the layer displacement *d* in the intervals *a* and *b* are presented in Figure 2, III, IV. Curves 1, 2, and 3 are A_a, A_p, and *d* as a function of the ray perigee height. Curves 4 indicate layer inclination angles δ in degrees (vertical scales to the right). Curves 5 are corrections Δ*h* [km] to the actual height *h′* of layers *a* (Figure 2, III) and *b* (Figure 2, IV). For the layers in the intervals *a* and *b*, values of the displacement *d* are from –630 to –800 km and from –600 to –750 km respectively (the interval *c* is omitted). According to (5), the statistical error in estimating the ratio $(A_a-A_p)/A_p$ is minimum at maximum A_p. If the relative measurement error in A_p is ~5%, then the accuracy of *d* estimate is ~±100 km. On the average, *d* = –730 km for the layer *a* and *d* = –620 km for the layer *b*. For the layer *c* the mean displacement is positive: *d* = 620 km. From Equation (6) we can find inclination angles δ of plasma layers *a*, *b*, and *c* with respect to the local horizon: −7.3°± 0.9°, −6.4°± 0.9°, and 6.4°± 0.9° respectively. We have also determined corrections Δ*h* to actual heights *h′* of the layers *a* (Δ*h* = 40 km), *b* (Δ*h* = 30 km), and *c* (Δ*h* = 30 km).

The local spherical symmetry allows us to use the Abel transform for solving the inverse problem and finding the distribution of electron density and its vertical gradient in the layer. The resulting dependence of the electron density $N_e(h')$ and its gradient dN_e/dh' are shown in Figures 3 and 4. We have restored vertical profiles of electron density and its vertical gradient for the layers *a*, *b*, and *c* from the radio occultation data on eikonal. The actual layer height *h′* and the ray perigee height *h* are shown respectively in the upper and lower horizontal axes of Figures 3 and 4.

Heights of electron density maxima for the layers are indicated by arrows (Figure 3). The comparison between Figures 2, I and 3 shows that the height of electron density maxima coincides with that of refraction attenuation minima for the layers *a*, *b*, and *c*. This is fully consistent with the simulation results [Zeng, Sokolovskiy, 2010]. When the radio wave propagation vector is parallel to the E_s-layer ionization plane, the passage of radio rays through the center of the layer (electron density peak)

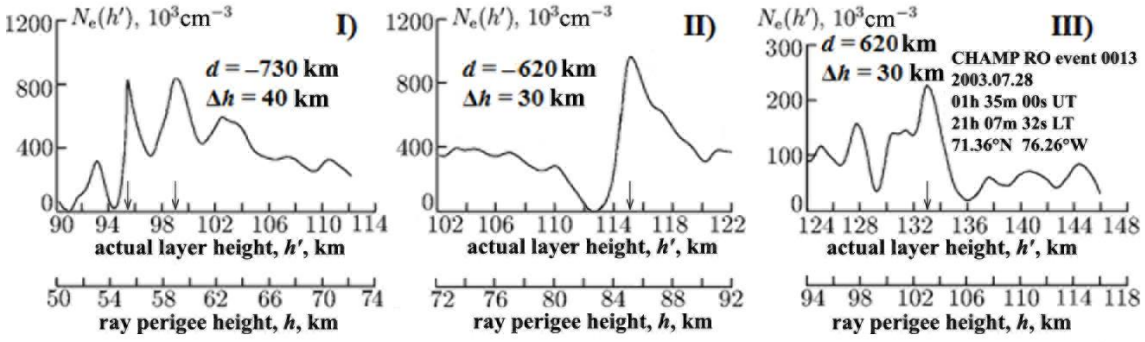

Figure 3. Electron density profiles for three ionospheric layers. Displacement, altitude correction, and angle of layer inclination are respectively: d = –730 km, Δh = 40 km, and δ = –7.3° (layer *a*, panel I); d = –620 km, Δh = 30 km, and δ = –6.4° (layer *b*, panel II); d = 620 km, Δh = 30 km, and δ = 6.4° (layer *c*, panel III). Heights of electron density maxima for the layers *a*, *b*, and *c* are indicated by arrows

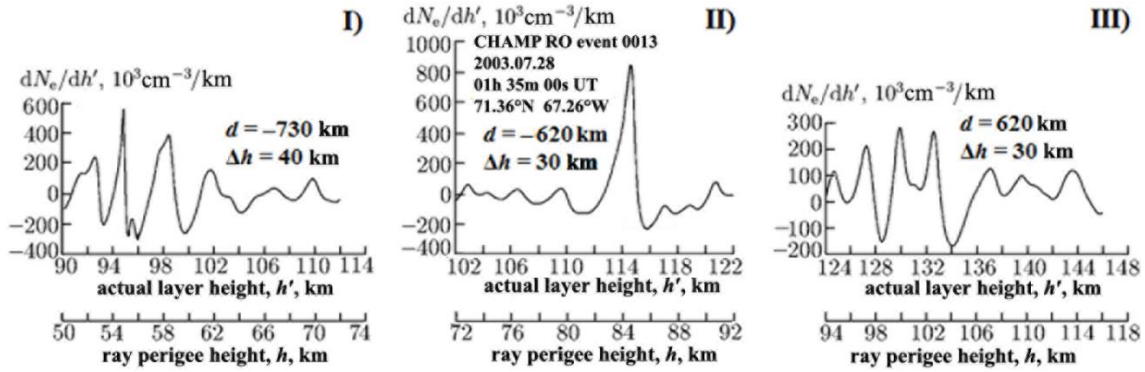

Figure 4. Profiles of the vertical gradient of electron density for ionospheric layers *a* (panel I), *b* (panel II), and *c* (panel III)

leads to defocusing; and through its edges, to focusing [Zeng, Sokolovskiy, 2010]. The layers *a* and *b* are located on TL (at 730 and 620 km from T respectively), with the electron density gradient maxima observed at 95.0 and 114.5 km (Figure 4, I, II). The layer *c* is located at a distance of 620 km from T on TG; and the vertical density gradient maximum, at a height of 130 km. Referring to Figure 4, the vertical gradient of electron density for the layers *a*, *b*, and *c* are within the following ranges:

$$-3.0 \cdot 10^5 \text{ cm}^{-3}/\text{km} < dN_e(h')/dh' < 5.6 \cdot 10^5 \text{ cm}^{-3}/\text{km},$$

$$-2.4 \cdot 10^5 \text{ cm}^{-3}/\text{km} < dN_e(h')/dh' < 8.5 \cdot 10^5 \text{ cm}^{-3}/\text{km},$$

$$-1.7 \cdot 10^5 \text{ cm}^{-3}/\text{km} < dN_e(h')/dh' < 2.8 \cdot 10^5 \text{ cm}^{-3}/\text{km}.$$

These values are typical for intense E_s layers in Earth's ionosphere observed by ground-based remote-sensing instruments, *in situ* methods, and satellite sensors [Whitehead, 1989; Mathews, 1998; Kelley, 2009]. The height range of RO-signal amplitude variations corresponds approximately to the range of variations in the electron density and its vertical gradient.

Figure 5 gives another example of the study of E_s layers in Earth's high-latitude ionosphere based on processing of CHAMP radio signals at f_1=1575.42 MHz (July 04, 2003, 02:27 UT; ray perigee coordinates 68.5°N, 82.8°W) in measurement session No. 26. The RO-signal refractive attenuations $X_a(h)$ and $X_p(h)$ derived from intensity and eikonal variations are shown in Figure 5, I as function of the ray perigee height h. In the height ranges 50–60 km and 75–85 km, the $X_a(h)$ and $X_p(h)$ variations are strongly correlated and can be regarded as coherent oscillations caused by the influence of sporadic layers (Figure 5, I, curves 1 and 2). The amplitudes A_a (Figure 5, II, III, curve 1) and A_p (Figure 5, II, III, curve 2) of analytical signals associated with $X_a(h)$ and $X_p(h)$ were calculated using the numerical Hilbert transform. In the height range 50–60 km, A_a is about 1.7 times lower than A_p.

According to Equation (5), here d is negative and the plasma layer is displaced from the ray perigee T to the satellite L (see Figure 1). The displacement d for the E_s layer assigned to a ray perigee height of 51 km is depicted in Figure 5, III (curve 3). Curve 3 shows d calculated from Equation (5) and A_a and A_p dependences in the height range 50.7–51.4 km. Values of d are concentrated in the range from –900 to –950 km, whereas the A_a and A_p functions vary within $0.7 \le A_a \le 0.75$ and $1.29 \le A_p \le 1.36$. If the relative measurement error in A_p is ~5 % (see Figure 5, III), the accuracy of d estimate is approximately ±120 km. The angle of inclination (δ = –8.2°±1.2°) of this plasma layer with respect to the local horizon was calculated from (6). For another layer, δ = –5.0°± 0.8°. The vertical gradient of electron density for the two ionospheric layers is shown in Figure 5, IV. Curves 1 and 2 correspond to the vertical gradient restored using Equations (12) and (16) from [Pavelyev et al., 2015]. Curve 3 is obtained using Formula (15) from [Pavelyev et al., 2015] and the refractive attenuation $X_a(h)$. The actual height of the ionospheric layers is represented on the horizontal axis in Figure 5, IV; their

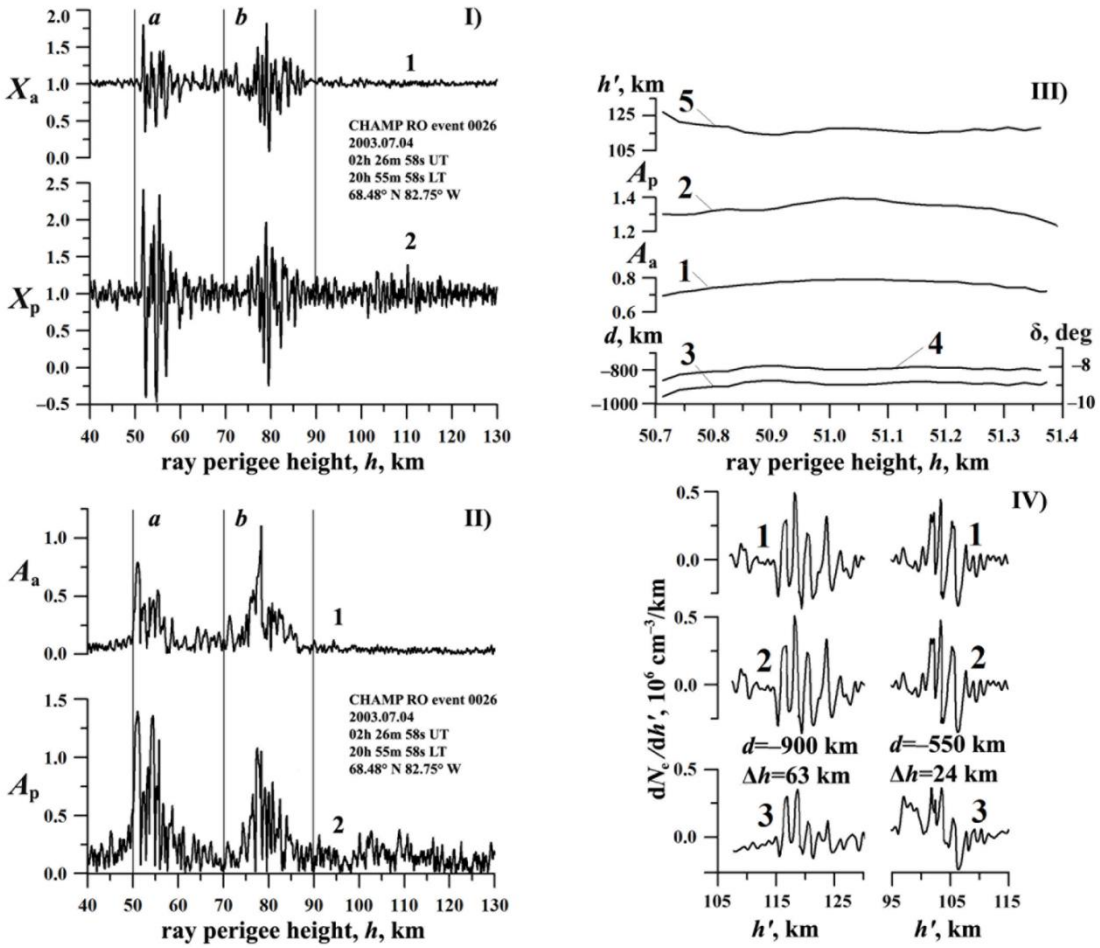

Figure 5. Refractive attenuations X_a and X_p obtained from CHAMP RO-signal intensity and eikonal variations at the GPS frequency f_1=1575.42 MHz (curves 1 and 2 in panel I respectively) in measurement session No. 26. Amplitudes A_a and A_p of analytical signals associated with X_a and X_p variations (curves 1 and 2 in panel II). Location, actual height, and inclination of layer *a* (panel III) determined by using A_a and A_p amplitudes of analytical signals (notations are the same as in Figure 2, III). Height profiles of the vertical gradient of electron density for two layers (panel IV) derived using Equations (12) and (16) from [Pavelyev et al., 2015] (curves 1 and 2 respectively) and Formula (15) from the same work, and of the refractive attenuation $X_a(h)$ (curve 3)

displacements *d* and height corrections Δ*h* are indicated in the legend. The first layer is on the line TL (height range 110–120 km) at a distance of ~900 km from the point T (Figure 5, IV, left). The second layer (95–105 km) is by ~550 km to the right of the ray perigee (Figure 5, IV, right). The comparison of the $X_a(h)$ and $X_p(h)$ variations (Figure 5, I, curves 1 and 2) and the vertical gradients of electron density (Figure 5, IV) suggests that the width of E_s layers corresponds approximately to the height range of RO-signal intensity variations.

MODULATION OF THE STRUCTURE OF E_S LAYERS BY INTERNAL ATMOSPHERIC WAVES

Propagation of internal gravity waves at ionospheric heights leads to the formation of ionization irregularities [Hines, 1960]. It is now known that internal atmospheric waves generate traveling ionospheric disturbances (TIDs) and sporadic E irregularities of several types. It has been established that TIDs feature a pronounced inclination of equal phase surfaces, whereas E_s layers exhibit nearly horizontal phase surfaces. This is due to the fact that E_s layers are formed by atmospheric tides and long-period buoyancy waves, which decay in the F-region of the ionosphere owing to dissipative effects [Gossard, Hooke, 1975]. According to the results obtained by Hines [1960], inclined fronts of TIDs should represent phase fronts of their associated buoyancy waves, and downward propagation of wave phase indicates upward propagation of IGW energy. Note that Otsuka et al. [2009] have shown that medium-scale TIDs may be generated by polarization electric fields. Most nighttime TIDs propagate southwestward, and this predominant propagation direction cannot be explained by the classical theory of internal gravity waves. Ionospheric instability acts through processes involving polarization electric fields, therefore it could also give rise to medium-scale TIDs [Otsuka et al., 2009]. Tsunoda and Cosgrove [2001] have studied the relationship between E_s layers and other ionospheric phenomena.

The internal atmospheric wave propagating through the ionosphere leads to the formation of a wave node of

ionization due to collisions between charged and neutral particles. Kato et al. [1970] have shown that the wave propagating through the E-region generates wave-like electron density variations, which have the same frequency and the same wave numbers as the initial IGW in the absence of boundaries or irregularities in the surrounding plasma. Chimonas and Axford [1968] have found that the wind shear leads to the formation of a wave node of ionization that moves down. This ionization shift from high levels to lower ones is known as the corkscrew effect. The role of small-scale internal waves that modulate the plasma layer formed by the tidal system has been discussed in [Chimonas, 1971]. The author has pointed out that if the IGW vertical phase speed is somewhat higher than the plasma layer drift speed and is downward, ions of the layer can "see" the wind structure of the virtually stationary wave that sweeps ions out through horizontal convergence/divergence zones, creating the characteristic "spottiness" of the E_s layer. Forced spatial resonance occurs when an ionization irregularity formed by some other method (e.g., atmospheric tide or long-period internal gravity wave) has a drift speed equal to the IGW phase speed. The original irregularity in this case should be situated so that it coincides with one of the ionization peaks produced by the atmospheric wave [Whitehead, 1971].

Internal atmospheric wave propagation modulates the structure of the initially horizontal E_s layer and causes the inclination of this layer with respect to the local horizon surface. We have developed a new method for determining characteristics of internal atmospheric waves associated with inclined sporadic structures in Earth's ionosphere. When restoring IGW parameters, we used the fundamental expressions (dispersion equation, polarization relationships, and definitions of wave characteristics) for IGWs [Gubenko et al., 2008, 2011, 2012, 2015, 2016a, b; Gubenko, Kirillovich, 2018]. This method allows us to examine the relationships between small-scale internal waves and E_s layers in Earth's ionosphere and significantly expands the capabilities of the traditional radio occultation monitoring of the atmosphere [Gubenko et al., 2018].

The idea of experimental determination of characteristics of the internal atmospheric wave associated with inclined plasma structures is as follows. A small-scale internal wave propagating through the E-region causes an E_s layer to incline, by turning its ionization plane parallel to the phase front of the internal wave. In this case, the angle δ between the wave propagation vector and the local vertical coincides with the inclination angle of the plasma E_s layer under study. To calculate characteristics of IGWs responsible for layer inclinations, we need background estimates of Brunt–Vaisala frequency (N_b) at the actual heights (h'), where the E_s layers *a*, *b*, and *c* are located (see Figures 2–4, measurement session No. 13). Since the data on N_b at heights of E_s layers is rather conservative, we have used the results for the reference atmosphere: N_b (h'=95 km) $\approx 2.3\cdot10^{-2}$ rad/s; N_b (h'=99 km) $\approx 2.2\cdot10^{-2}$ rad/s; N_b (h'=115 km) $\approx 2.1\cdot10^{-2}$ rad/s [Gossard, Hooke, 1975]. These values of buoyancy frequency N_b correspond to the periods τ_b ($\tau_b = 2\pi/N_b$) from 4.6 to 5.0 min, which agrees with the vertical profile of the period τ_b calculated for the standard atmosphere (refer to [Kelley, 2009], Figure 6.5). From the results shown in Figure 6.5 of [Kelley, 2009], we have also found that N_b (h' = 133 km) $\approx 2.3\cdot10^{-2}$ rad/s. Using these estimates and the experimental data, we have established that $1 >> \tan^2\delta$ and $\omega^2 >> f^2$. Given these inequalities, the dispersion equation and the expressions for wave characteristics take a very simple form [Gubenko et al., 2018]:

$$\begin{aligned} &\omega / N_b = \lambda_z / \lambda_h = |\tan\delta|, \ \tau_i = 2\pi/\omega, \\ &\left|c_{ph}^{in}\right| = \omega / |k_h| = N_b / |m|, \\ &\left|c_{pz}^{in}\right| = \omega / |m| = N_b |\tan\delta| / |m|, \end{aligned} \quad , \qquad (7)$$

where ω is the IGW intrinsic frequency; τ_i is the intrinsic period of an internal wave; $k_h = 2\pi/\lambda_h$ and $m = 2\pi/\lambda_z$ are the horizontal and vertical wave numbers; λ_h and λ_z are the horizontal and vertical wavelengths; c_{ph}^{in} and c_{pz}^{in} are the intrinsic horizontal and vertical phase speeds. From (7) we can calculate characteristics of the small-scale internal waves that are responsible for inclinations of initially horizontal E_s layers in Earth's ionosphere (CHAMP RO measurement session No. 13):

Layer *a* (bottom) (h'= 95 km, Δh = 40 km): λ_z = 3.0 km; $\delta = -7.3°$; $|\tan\delta| = 0.13$; λ_h = 23.1 km; $\left|c_{ph}^{in}\right|$ = 11.0 m/s; $\left|c_{pz}^{in}\right|$ = 1.4 m/s; $N_b = 2.3\cdot10^{-2}$ rad/s; $\omega = 3.0\cdot10^{-3}$ rad/s; τ_i = 34.9 min.

Layer *a* (top) (h'= 99 km, Δh=40 km): λ_z=4.4 km; $\delta = -7.3°$; $|\tan\delta| = 0.13$; λ_h=33.8 km; $\left|c_{ph}^{in}\right|$ = 15.4 m/s; $\left|c_{pz}^{in}\right|$ = 2.0 m/s; $N_b = 2.2\cdot10^{-2}$ rad/s; $\omega = 2.9\cdot10^{-3}$ rad/s; τ_i = 36.1 min.

Layer *b* (h' = 115 km, Δh = 30 km): λ_z = 4.4 km; $\delta = -6.4°$; $|\tan\delta| = 0.11$; λ_h = 40.0 km; $\left|c_{ph}^{in}\right|$ = 14.7 m/s; $\left|c_{pz}^{in}\right|$ = 1.6 m/s; $N_b = 2.1\cdot10^{-2}$ rad/s; $\omega = 2.3\cdot10^{-3}$ rad/s; τ_i = 45.5 min.

Layer *c* (h' = 133 km, Δh = 30 km): λ_z = 3.0 km; $\delta = 6.4°$; $|\tan\delta| = 0.11$; λ_h = 27.3 km; $\left|c_{ph}^{in}\right|$ = 11.0 m/s; $\left|c_{pz}^{in}\right|$ = 1.2 m/s; $N_b = 2.3\cdot10^{-2}$ rad/s; $\omega = 2.5\cdot10^{-3}$ rad/s; τ_i = 41.9 min.

Let us also present the characteristics of internal atmospheric waves modulating E_s layers in Earth's ionosphere, which we recorded in measurement session No. 26:

Layer *a* (h'=114 km, Δh=63 km): λ_z=2.5 km; δ= –8.2°; $|\tan\delta| = 0.14$; λ_h = 17.9 km; $\left|c_{ph}^{in}\right|$ = 8.2 m/s; $\left|c_{pz}^{in}\right|$ = 1.2 m/s; $N_b = 2.1\cdot10^{-2}$ rad/s; $\omega = 2.9\cdot10^{-3}$ rad/s; τ_i = 36.1 min.

Layer *b* (h' = 99 km, Δh = 24 km): λ_z = 2.0 km; $\delta = -5.0°$; $|\tan\delta| = 0.09$; λ_h = 23.0 km; $\left|c_{ph}^{in}\right|$ = 7.4 m/s; $\left|c_{pz}^{in}\right|$ = 0.6 m/s; $N_b = 2.2\cdot10^{-2}$ rad/s; $\omega = 2.0\cdot10^{-3}$ rad/s; τ_i = 52.3 min.

It is important that the IGW intrinsic frequency and period can be determined given only Brunt-Vaisala frequency (N_b) and the angle (δ) between wave propagation vector and local vertical. The intrinsic period of the internal waves under study is from 35 to 46 min, and the IGW intrinsic vertical phase speed ranges from 1.2 to 2.0 m/s (measurement session No. 13). The resulting estimates are in good agreement with the ~ 30 min periods and <2.0 m/s vertical wind speed at an altitude of ~100 km (in the ground-based reference system) calculated for the model of E_s layer in the polar cap [MacDougall et al., 2000a, b]. Note that the vertical wind shear nodes, in which the wind speed is zero, coincide with the location of E_s layers, therefore the IGW intrinsic period should coincide with the wave period measured in the ground-based system [Gubenko, Kirillovich, 2018]. Thus, the characteristics of internal atmospheric waves we restored are fully consistent with the results of independent research and simulated data on Earth's high-latitude ionosphere [Kirkwood, Collis, 1989; Turunen et al., 1993; Heinselman et al., 1998; MacDougall et al., 2000a, b].

CONCLUSION

We have developed a method for determining characteristics of internal atmospheric waves, which relies on the use of inclined ionospheric sporadic E layers as a detector. The method is based on the fact that an internal wave propagating through an initially horizontal E_s layer causes plasma density gradient to rotate in the direction of the wave vector and the layer ionization plane to turn parallel to the phase wave front. This method allows us to examine relationships between small-scale internal waves and E_s layers in Earth's ionosphere and significantly expands the capabilities of the traditional radio occultation monitoring of the atmosphere. The obtained periods (from 35 to 46 min) and vertical phase speeds (from 1.2 to 2.0 m/s) of internal atmospheric waves agree well with the results of independent experiments and simulated data on sporadic E-structures at an altitude of ~100 km in Earth's polar cap.

The work was performed in the framework of the State Task and partially supported by the Russian Foundation for Basic Research (RFBR project No.19-02-00083 A) and RAS Presidium Program No. 12.

REFERENCES

Arras C., Wickert J., Beyerle G., Heise S., Schmidt T., Jacobi C. A global climatology of ionospheric irregularities derived from GPS radio occultation. *Geophys. Res. Lett.* 2008, vol. 35, no.L14809. DOI: 10.1029/2008GL03415.

Bernhardt P.A. The modulation of sporadic-E layers by Kelvin—Helmholtz billows in the neutral atmosphere. *J. Atmos. Solar-Terr. Phys*. 2002, vol. 64, pp. 1487–1504.

Bernhardt P.A., Selcher C.A., Siefring C., Wilkens M., Compton C., Bust G. Yamamoto M., Fukao S., Takayuki O., Wakabayashi M., Mori H. Radio tomographic imaging of sporadic-E layers during SEEK-2. *Ann. Geophys*. 2005, vol. 23, pp. 2357–2368. DOI: 10.5194/angeo-23-2357-2005.

Bristow W.A., Watkins B.J. Numerical simulation of the formation of thin ionization layers at high latitudes. *Geophys. Res. Lett*. 1991, vol. 18, pp. 404–407.

Bristow W.A., Watkins B.J. Incoherent scatter observations of thin ionization layers at Sondrestrom. *J. Atmos. Terr. Phys*. 1993, vol. 55, pp. 873–894.

Chimonas G., Axford W.I. Vertical movement of temperate-zone sporadic E layers. *J. Geophys. Res.* 1968, vol. 73, pp. 111–117.

Chimonas G. Enhancement of sporadic E by horizontal transport within the layer. *J. Geophys. Res*. 1971, vol. 76, pp. 4578–4586.

Chu Y.-H., Brahmanandam P.S., Wang C.-Y., Ching-Lun S., Kuong R.-M. Coordinated sporadic E layer observations made with Chung-Li 30 MHz radar, ionosonde and FORMOSAT-3/COSMIC satellites. *J. Atmos. Solar-Terr. Phys*. 2011, vol. 73, pp. 883–894. DOI: 10.1016/j.jastp.2010.10.004.

Cosgrove R.B., Tsunoda R.T. A direction-dependent instability of sporadic-E layers in the nighttime midlatitude ionosphere. *Geophys. Res. Lett*. 2002, vol. 29, no. 18. 1864. DOI: 10.1029/2002GL014669.

Cosgrove R.B., Tsunoda R.T. Instability of the E-F coupled nighttime midlatitude ionosphere. *J. Geophys. Res*. 2004, vol. 10, no. A04305. DOI: 10.1029/2003JA010243.

Cox R.M., Plane J.M.C. An ion-molecule mechanism for the formation of neutral sporadic Na layers. *J. Geophys. Res.* 1998, vol. 103, no. D6, pp. 6349–6359. DOI: 10.1029/97JD03376.

Didebulidze G.G., Lomidze L.N. Double atmospheric gravity wave frequency oscillations of sporadic E formed in a horizontal shear flow. *Phys. Lett. A.* 2010, vol. 374, no. 7. pp. 952–969. DOI: 10.1016/j.physleta.2009.12.026.

Gossard E.E, Hooke W.H. *Waves in the Atmosphere.* Amsterdam, Oxford, New York, Elsevier Scientific Publishing Co., 1975, 471 p.

Gubenko V.N., Kirillovich I.A. Diagnostics of internal atmospheric wave saturation and determination of their characteristics in Earth's stratosphere from radiosonde measurements. *Solar-Terr. Phys.* 2018, vol. 4, no. 2, pp. 41–48. DOI: 10.12737/stp-42201807.

Gubenko V.N., Pavelyev A.G., Andreev V.E. Determination of the intrinsic frequency and other wave parameters from a single vertical temperature or density profile measurement. *J. Geophys. Res*. 2008. vol. 113, no. D08109. DOI: 10.1029/2007JD008920.

Gubenko V.N., Pavelyev A.G., Salimzyanov R.R., Pavelyev A.A. Reconstruction of internal gravity wave parameters from radio occultation retrievals of vertical temperature profiles in the Earth's atmosphere. *Atmos. Meas. Tech*. 2011, vol. 4, no. 10, pp. 2153–2162. DOI: 10.5194/amt-4-2153-2011.

Gubenko V.N., Pavelyev A.G., Salimzyanov R.R., Andreev V.E. A method for determination of internal gravity wave parameters from a vertical temperature or density profile measurement in the Earth's atmosphere. *Cosmic Res*. 2012, vol. 50, no. 1, pp. 21–31. DOI: 10.1134/S0010952512010029.

Gubenko V.N., Kirillovich I.A., Pavelyev A.G. Characteristics of internal waves in the Martian atmosphere obtained on the basis of an analysis of vertical temperature profiles of the Mars Global Surveyor mission. *Cosmic Res*. 2015, vol. 53, no. 2, pp. 133–142. DOI: 10.1134/S0010952515020021.

Gubenko V.N., Kirillovich I.A. Pavelyev A.G., Andreev V.E. Detection of saturated internal gravity waves and reconstruction of their characteristics in the Martian atmosphere. *Izvestiya vysshikh uchebnykh zavedenii. Fizika* [Russian Physics Journal]. 2016a, vol. 59, no. 12-2, pp. 46–49. (In Russian).

Gubenko V.N., Kirillovich I.A., Liou Y.-A., Pavelyev A.G. Monitoring of internal gravity waves in the Arctic and Antarctic atmosphere. *Izvestiya vysshikh uchebnykh zavedenii. Fizika* [Russian Physics Journal]. 2016b, vol. 59, no. 12-3, pp. 80–85. (In Russian).

Gubenko V.N., Pavelyev A.G., Kirillovich I.A., Liou Y.-A. Case study of inclined sporadic E layers in the Earth's ionosphere observed by CHAMP/GPS radio occultations: Coupling between the tilted plasma layers and internal waves. *Adv. Space Res.* 2018,

vol. 61, no 7, pp. 1702–1716. DOI: 10.1016/j.asr.2017.10.001.

Haldoupis C.A. Tutorial review on sporadic E layers. *Aeronomy of the Earth's Atmosphere and Ionosphere.* Berlin, Springer, 2011, pp. 381–394. (IAGA Special Sopron Book Series 2). DOI: 10.1007/978-94-007-0326-1-2.

Haldoupis C. Midlatitude sporadic E layers. A typical paradigm of atmosphere–ionosphere coupling. *Space Sci. Rev*. 2012, vol. 168, pp. 441–461. DOI: 10.1007/s11214-011-9786-8.

Heinselman C.J., Thayer J.P., Watkins B.J. A high-latitude observation of sporadic sodium and sporadic E-layer formation. *Geophys. Res. Lett*. 1998, vol. 25, pp. 3059–3062. DOI: 10.1029/98GL02215.

Hines C.O. Internal atmospheric gravity waves at ionospheric heights. *Can. J. Phys*. 1960, vol. 38, pp. 1441–1481.

Hunten D.M., Turco R.P., Toon O.B. Smoke and dust particles of meteoric origin in the mesosphere and stratosphere. *J. Atmos. Sci*. 1980, vol. 37, pp. 1342–1357.

Hysell D.L., Yamamoto M., Fukao S. Imaging radar observations and theory of type I and type II quasi-periodic echoes. *J. Geophys. Res*. 2002, vol. 107, no. A11, 1360. DOI: 10.1029/2002JA009292.

Hysell D.L., Larsen M.F., Zhou Q.H. Common volume coherent and incoherent scatter radar observations of mid-latitude sporadic E-layers and QP echoes. *Ann. Geophys*. 2004, vol. 22, pp. 3277–3290. DOI: 10.5194/angeo-22-3277-2004.

Hysell D.L., Nossa E., Larsen M.F., Munro J., Sulzer M.P., González S.A. Sporadic E layer observations over Arecibo using coherent and incoherent scatter radar: Assessing dynamic stability in the lower thermosphere. *J. Geophys. Res*. 2009, vol. 114, no. A12303. DOI: 10.1029/2009JA014403.

Igarashi K., Pavelyev A.G., Hocke K., Pavelyev D., Wickert J. Observation of wave structures in the upper atmosphere by means of radio holographic analysis of the radio occultation data. *Adv. Space Res*. 2001, vol. 27, pp. 1321–1327. DOI: 10.1016/s0273-1177(01)00144-2.

Kato S., Reddy C.A., Matsushita S. Possible hydromagnetic coupling between the perturbations of the neutral and ionized atmosphere. *J. Geophys. Res*. 1970, vol. 75, pp. 2540–2550.

Kelley M.C. *The Earth's Ionosphere: Plasma Physics and Electrodynamics*. Second Edition. San Diego, Academic Press, 2009, 556 p.

Kirkwood S., Collis P.N. Gravity wave generation of simultaneous auroral sporadic-E layers and sudden neutral sodium layers. *J. Atmos. Terr. Phys*. 1989, vol. 51, no. 4, pp. 259–269.

Kirkwood S., von Zahn U. On the role of auroral electric fields in the formation of low altitude sporadic-E and sudden sodium layers. *J. Atmos. Terr. Phys*. 1991, vol. 53, pp. 389–407.

Kirkwood S., von Zahn U. Formation mechanisms for lowaltitude Es and their relationship with neutral Fe layers: Results from the METAL campaign. *J. Geophys. Res*. 1993, vol. 98, pp. 21549–21561.

Kirkwood S., Nilsson H. High-latitude sporadic-E and other thin layers — the role of magnetospheric electric fields. *Space Sci. Rev*. 2000, vol. 91, pp. 579–613. DOI: 10.1023/A:1005241931650.

Larsen M.F. A shear instability seeding mechanism for quasiperiodic radar echoes. *J. Geophys. Res*. 2000, vol. 105, no. A11, pp. 24931–24940. DOI: 10.1029/1999JA000290.

Larsen M.F., Fukao S., Yamamoto M., Tsunoda R., Igarashi K., Ono T. The SEEK chemical release experiment: Observed neutral wind profile in a region of sporadic-E. *Geophys. Res. Lett*. 1998, vol. 25, pp. 1789–1792. DOI: 10.1029/98GL00986.

Larsen M.F., Yamamoto M., Fukao S., Tsunoda R.T. SEEK 2: Observations of neutral winds, wind shears, and wave structure during a sporadic E/QP event. *Ann. Geophys*. 2005, vol. 23, pp. 2369–2375. DOI: 10.5194/angeo-23-2369-2005.

Larsen M.F., Hysell D.L., Zhou Q.H., Smith, S.M., Friedman, J., Bishop, R.L. Imaging coherent scatter radar, incoherent scatter radar, and optical observations of quasiperiodic structures associated with sporadic E layers. *J. Geophys. Res*. 2007, vol. 112, no. A06321. DOI: 10.1029/2006JA012051.

Lehmacher G.A., Larsen M.F., Croskey C.L. Observation of electron biteout regions below sporadic E layers at polar latitudes. *Ann. Geophys*. 2015, vol. 33, pp. 371–380. DOI: 10.5194/angeo-33-371-2015.

MacDougall J.W., Jayachandran P.T., Plane J.M.C. Polar cap sporadic-E: part 1, observations. *J. Atmos. Solar-Terr. Phys*. 2000a, vol. 62, pp. 1155–1167. DOI: 10.1016/S1364-6826(00)00093-6.

MacDougall J.W., Plane J.M.C., Jayachandran P.T. Polar cap sporadic-E: part 2, modeling. *J. Atmos. Solar-Terr. Phys*. 2000b, vol. 62, pp. 1169–1176. DOI: 10.1016/S1364-6826(00)00092-4.

Malhotra A., Mathews J.D., Urbina J. Effect of meteor ionization on sporadic-E observed at Jicamarca. *Geophys. Res. Lett*. 2008, vol. 35, L15106. DOI: 10.1029/2008GL034661.

Maruyama T., Fukao S., Yamamoto M. A possible mechanism for echo striation generation of radar backscatter from midlatitude sporadic E. *Radio Sci*. 2000, vol. 35, pp. 1155–1164. DOI: 10.1029/1999RS002296.

Maruyama T., Kato H., Nakamura M. Ionospheric effects of the Leonid meteor shower in November 2001 as observed by rapid run ionosondes. *J. Geophys. Res*. 2003, vol. 108, no. A8. 1324. DOI: 10.1029/2003JA009831.

Maruyama T., Kato H., Nakamura M. Meteor-induced transient sporadic E as inferred from rapid-run ionosonde observations at midlatitudes. *J. Geophys. Res*. 2008, vol. 113, no. A09308. DOI: 10.1029/2008JA013362.

Mathews J.D. Sporadic E: Current views and recent progress. *J. Atmos. Solar-Terr. Phys*. 1998, vol. 60, no. 4, pp. 413–435. DOI: 10.1016/S1364-6826(97)00043-6.

Nygren T., Jalonen L., Oksman J., Turunen T. The role of electric field and neutral wind direction in the formation of sporadic E-layers. *J. Atmos. Terr. Phys*. 1984, vol. 46, pp. 373–381.

Ogawa T., Takahashi O., Otsuka Y., Nozaki K., Yamamoto M., Kita K. Simultaneous middle and upper atmosphere radar and ionospheric sounder observations of midlatitude E region irregularities and sporadic E layer. *J. Geophys. Res*. 2002, vol. 107, no. A10, 1275. DOI: 10.1029/2001JA900176.

Otsuka Y., Shiokawa K., Ogawa T., Yokoyama T., Yamamoto M. Spatial relationship of nighttime medium-scale traveling ionospheric disturbances and F region field-aligned irregularities observed with two spaced all-sky airglow imagers and the middle and upper atmosphere radar. *J. Geophys. Res*. 2009, vol. 114, no. A05302. DOI: 10.1029/2008JA013902.

Pavelyev A.G., Liou Y.A., Wickert J., Gubenko V.N., Pavelyev A.A., Matyugov S.S. New applications and advances of the GPS Radio Occultation Technology as recovered by analysis of the FORMOSAT-3/COSMIC and CHAMP data-base. *New Horizons in Occultation Research: Studies in Atmosphere and Climate*. Berlin, Heidelberg, Springer-Verlag, 2009, pp. 165–178. DOI: 10.1007/978-3-642-00321_9.

Pavelyev A.G., Liou Y.A., Zhang K., Wang C.S., Wickert J., Schmidt T., Gubenko V.N., Pavelyev A.A., Kuleshov Y. Identification and localization of layers in the ionosphere using the eikonal and amplitude of radio occultation signals. *Atmos. Meas. Tech*. 2012, vol. 5, no. 1, pp. 1–16. DOI: 10.5194/amt-5-1-2012.

Pavelyev A.G., Liou Y.A., Matyugov S.S., Pavelyev A.A., Gubenko V.N., Zhang K., Kuleshov Y. Application of the locality principle to radio occultation studies of the Earth's atmosphere and ionosphere. *Atmos. Meas. Tech*. 2015, vol. 8, no. 7, pp. 2885–2899. DOI: 10.5194/amt-8-2885-2015.

Roddy P.A. Earle G.D., Swenson C.M., Carlson C.G., Bullett T.W. Relative concentrations of molecular and metallic ions in midlatitude intermediate and sporadic-E layers.

Geophys. Res. Lett. 2004, vol. 31, no. L19807. DOI: 10.1029/2004 GL020604.

Saito S., Yamamoto M., Hashiguchi H., Maegawa A. Observation of three-dimensional structures of quasi-periodic echoes associated with mid-latitude sporadic-E layers by MU radar ultra-multi-channel system. *Geophys. Res. Lett*. 2006, vol. 33, no. L14109. DOI: 10.1029/2005GL025526.

Tsunoda R.T., Cosgrove R.B. Coupled electrodynamics in the nighttime midlatitude ionosphere . *Geophys. Res. Lett*. 2001, vol. 8, pp. 4171–4174. DOI: 10.1029/2001GL013245.

Tsunoda R.T., Fukao S. Yamamoto M. On the origin of quasiperiodic radar backscatter from midlatitude sporadic E. *Radio Sci*. 1994, vol. 29, pp. 349–366.

Turunen T., Nygren T., Huuskonen A. Nocturnal high-latitude E-region in winter during extremely quiet conditions. *J. Atmos. Terr. Phys*. 1993, vol. 55, pp. 783–795.

Whitehead J.D. Ionization disturbances caused by gravity waves in the presence of an electrostatic field and background wind. *J. Geophys. Res*, 1971. vol. 76, pp. 238–241.

Whitehead J.D. Recent work on midlatitude and equatorial sporadic E. *J. Atmos. Terr. Phys*. 1989, vol. 51, pp. 401–424. DOI: 10.1016/0021-9169(89)90122-0.

Woodman R.F., Yamamoto M., Fukao S. Gravity wave modulation of gradient drift instabilities in mid-latitude sporadic E irregularities. *Geophys. Res. Lett*. 1991, vol. 18, pp. 1197–1200. DOI: 10.1029/91GL01159.

Wu D.L., Ao C.O., Hajj G.A., de la Torre Juarez M., Mannucci A.J. Sporadic E morphology from GPS-CHAMP radio occultations. *J. Geophys. Res*. 2005, vol. 110, no. A01306. DOI: 10.1029/2004JA010701.

Yamamoto M., Fukao S., Ogawa T., Tsuda T., Kato S. A morphological study of mid-latitude E-region field-aligned irregularities observed with the MU radar. *J. Atmos. Solar-Terr. Phys*. 1992, vol. 54, pp. 769–777.

Yamamoto M., Fukao S., Tsunoda R.T., Pfaff R., Hayakawa H. SEEK-2 (Sporadic-E Experiment over Kyushu 2) — Project Outline, and Significance. *Ann. Geophys*. 2005, vol. 23, pp. 2295–2305. DOI: 10.5194/angeo-23-2295-2005.

Yamamoto M., Fukao S., Woodman R.F., Ogawa T., Tsuda T., Kato K. Mid-latitude E region field-aligned irregularities observed with the MU radar. *J. Geophys. Res.: Space*. 1991, vol. 96, pp. 15943–15949.

Yokoyama T., Yamamoto M., Fukao S., Cosgrove R.B. Three-dimensional simulation on generation of polarization electric field in the midlatitude E-region ionosphere. *J. Geophys. Res*. 2004, vol. 109, no. A01309. DOI: 10.1029/2003JA010238.

Yokoyama T., Yamamoto M., Fukao S., Takahashi T., Tanaka M. Numerical simulation of mid-latitude ionospheric E-region based on SEEK and SEEK-2 observations. *Ann. Geophys*. 2005, vol. 23, no. 7, pp. 2377–2384. DOI: 10.5194/angeo-23-2377-2005.

Yokoyama T., Hysell D.L., Otsuka Y., Yamamoto M. Three-dimensional simulation of the coupled Perkins and Es-layer instabilities in the nighttime midlatitude ionosphere. *J. Geophys. Res*. 2009, vol. 114, no. A03308. DOI: 10.1029/2008JA013789.

Yue X., Schreiner W.S., Zeng Z., Kuo Y.-H., Xue X. Case study on complex sporadic E layers observed by GPS radio occultations. *Atmos. Meas. Tech*. 2015, vol. 8, pp. 225–236. DOI: 10.5194/amt-8-225-2015.

Zeng Z., Sokolovskiy S. Effect of sporadic E cloud on GPS radio occultation signal. *Geophys. Res. Lett*. 2010, vol. 37, no. L18817. DOI: 10.1029/2010GL044561.

How to cite this article

Gubenko V.N., Kirillovich I.A. Modulation of sporadic E layers by small-scale atmospheric waves in Earth's high-latitude ionosphere. *Solar-terrestrial physics*. 2019. Vol. 5. Iss. 3. P. 98–108. DOI: 10.12737/stp-53201912.